(29) Katz, J. R. *Trans. Faraday Soc.* **1936**, *32*, 77.
(30) Miller, R. L.; Boyer, R. F.; Heijboer, J. *J. Polym. Sci., Polym. Phys. Ed.* **1984**, *22*, 2021.
(31) Tool, A. Q.; Eichlin, C. G. *J. Am. Ceramic Soc.* **1931**, *14*, 276.
(32) Ricco, T.; Smith, T. L. *Polymer* **1985**, *26*, 1979.
(33) Smith, T. L.; Ricco, T.; Levista, G.; Moonan, W. K. *Plast. Rubber Process. Appl.* **1986**, *6*, 81.
(34) Weitz, A.; Wunderlich, B. *J. Polym. Sci., Polym. Phys. Ed.* **1974**, *12*, 2473.
(35) Prest, W. M., Jr.; Roberts, F. J., Jr. *Ann. N. Y. Acad. Sci.* **1981**, *371*, 67.
(36) Bracewell, R. N. *The Fourier Transform and Its Applications*, 2nd ed.; McGraw-Hill: New York, 1978; p 113.
(37) Kohler, F. *The Liquid State*; Verlag Chemie: Weinheim, Germany, 1972; Chapter 4.
(38) Fisher, I. Z.; Adamovich, V. I. *J. Struct. Chem. USSR (Engl. Transl.)* **1963**, *4*, 759.
(39) Chay, T. R.; Frank, H. S. *J. Chem. Phys.* **1972**, *57*, 2910.

A Surface Light Scattering Study of Poly(ethylene oxide) and Poly(vinyl acetate) at the Air/Water and Heptane/Water Interfaces

Bryan B. Sauer, Masami Kawaguchi,† and Hyuk Yu*

Department of Chemistry, University of Wisconsin, Madison, Wisconsin 53706.
Received April 2, 1987

ABSTRACT: Spread films of poly(ethylene oxide) (PEO) and poly(vinyl acetate) (PVAc) were studied at the interfaces of air/water (A/W) and heptane/water (O/W) by using the Wilhelmy plate method for static surface tension measurements and the surface quasi-elastic light scattering (SLS) method for deducing the dynamic surface viscoelastic parameters. Upon effecting precise measurements at A/W, we show that the surface dilational elasticity determined from the Wilhelmy plate method and the longitudinal elasticity deduced from SLS were the same for a wide surface concentration range. The surface longitudinal viscosity of PEO films was shown to be less than that of PVAc films by a factor of 10 or more. To our knowledge, this is the first report of a study of homopolymers spread as films on any oil/water interface by the SLS technique. We have found that the surface pressure can be calculated from the SLS data because of the decoupling of the longitudinal waves from the transverse capillary waves. The dynamic surface pressure thus obtained agreed with the static surface pressure determined by the Wilhelmy method over the whole concentration range of PVAc. The transverse viscosity could also be calculated exactly for PEO and PVAc and was found to be close to zero in both cases.

Introduction

Interfacial activity of a water-soluble polymer, poly(ethylene oxide) (PEO), is an interesting subject[1,2] which also commands significant technological implications because many nonionic surfactants contain the ethylene oxide moiety. Although experiments with spread films of PEO at the air/water interface (henceforth denoted as A/W for short) have been published,[1,2] those on oil/water interfaces are yet to be found in the literature. On the other hand, studies of adsorbed films at O/W as contrasted to spread films have been reported.[3,4] Some reviews[5,6] covering a wide range of surface-active polymers are available in the literature. This is the second[7] in a series of papers comparing surface-active polymeric materials at A/W and at the heptane–water interface (henceforth denoted as O/W) by the surface quasi-elastic light scattering (SLS) technique. The purpose of this paper is twofold. We present the results of SLS experiments, performed at A/W with sufficient precision to allow a quantitative comparison of film elasticities obtained by SLS and the static Wilhelmy plate method. Further, upon making minor optical modifications of the SLS instrument, ready access to the oil/water interface has been accomplished.[7,8] The experiments on homopolymer films at O/W serve to elucidate the advantages and disadvantages of the SLS technique at O/W compared to A/W.

The SLS technique has only begun to be exploited for polymeric films. It has a potential of providing a new set of approaches to polymeric monolayers and films on various interfaces. Recently, there has been an active interest at A/W with respect to small molecule amphiphiles[9-14] such as fatty acids using SLS, but the interpretation of any viscoelastic parameters extracted from SLS is complicated by the various phase transitions and also by the fact that small molecule amphiphile monolayers are inherently less stable than polymer monolayers.[6] Thus, we have also chosen to study poly(vinyl acetate) (PVAc) because it forms stable films of the "expanded type", in addition to PEO for comparison sake.

Some of the questions which must be answered before SLS can be accepted as a well-validated technique deal with the interpretation of viscoelastic parameters; how to compare them with the results of other techniques and deciding which film viscoelastic parameters can actually be extracted by SLS. For film-covered surfaces there is an inherent coupling between the longitudinal (containing shear and dilational components[15]) waves and transverse capillary waves. For film-free liquid interfaces, the capillary wave motion is governed completely by the interfacial tension and the densities and viscosities of the two phases. With a film present, the situation becomes more complicated. An additional film viscoelastic parameter[12] is defined by making the surface tension complex, i.e., $\sigma^* = \sigma - i\omega\mu$, where μ is the transverse surface viscosity and $\omega = 2\pi f_s - i2\pi(\Delta f_{s,c}/2)$, f_s and $\Delta f_{s,c}$ being the frequency shift and corrected frequency full width at half-height, respectively, of the power spectrum of scattered light. Even though the longitudinal waves have a negligible contribution to the light scattering intensity, these waves couple with the transverse capillary waves. The longitudinal waves are governed by a complex elasticity, $\epsilon^* = \epsilon - i\omega\kappa$ where ϵ and κ are the longitudinal elasticity and viscosity, respectively. The longitudinal elasticity ϵ contains a shear component as stated above which cannot be separated

† Permanent address: Department of Industrial Chemistry, Faculty of Engineering, Mie University, Tsu, Mie 514, Japan.

0024-9297/87/2220-2732$01.50/0

from the dilational part by SLS.[15] Goodrich has given plausible physical pictures of the above-mentioned viscoelastic parameters.[16]

To provide an idea of the dependence of the two experimental quantities f_s and $\Delta f_{s,c}$ on the viscoelastic parameters, Hård and Löfgren[9] have calculated f_s and $\Delta f_{s,c}$ as functions of ϵ and κ at A/W. According to their calculations, f_s is weakly dependent on ϵ whereas $\Delta f_{s,c}$ is strongly dependent. For example, $\Delta f_{s,c}$ increases by almost 200% at a value of the reduced elasticity $\epsilon/\sigma = 0.2$, which is just the ratio of the longitudinal elasticity to the surface tension. The dependence of f_s and $\Delta f_{s,c}$ on the other film viscoelastic parameter μ has also been calculated by Langevin.[12]

Similar calculations can be done at the oil/water interfaces with two additional quantities, the viscosity and density of the second phase. Solving the dispersion relation with six input parameters (the densities and bulk shear viscosities of the two liquids and the scattering wave vector $\mathbf{k}$ and the interfacial tension σ), one obtains the dependence of f_s and $\Delta f_{s,c}$ on ϵ at different values of κ and μ. These calculations were presented earlier[7] for $\mathbf{k} = 459$ cm^{-1} and $\sigma = 50.83$ dyn/cm at O/W where the independent variable is expressed as the reduced longitudinal elasticity ϵ/σ. Since the densities and viscosities of the two phases are comparable at O/W, there exists negligible coupling between the longitudinal waves and transverse waves.[17] This was clearly illustrated by the above-mentioned calculations. In the most sensitive case, i.e., $\kappa = 0$, $\Delta f_{s,c}$ is changed only by about 8% as the coupling becomes progressively more efficient from the bare interface, i.e., $\epsilon/\sigma = 0$, to the maximal extent when the reduced elasticity reaches a value of 0.2. At A/W, the maximal change in $\Delta f_{s,c}$ comes to almost 200%. These calculations also indicate that f_s is mildly affected by ϵ/σ, which is not very different from A/W. Predictions of the dispersion relation[7] also indicated that μ, if present, could have a large effect on the light scattering spectrum, which is rather similar to the predicted effect for A/W.[12]

Finally, we address some of the questions raised in the literature dealing with film viscoelasticity. Before doing so, we designate the *dynamic* viscoelastic parameters as those extracted from SLS measurements. There is still a controversy dealing with the question of whether the dynamic transverse surface viscosity even exists at A/W. In Langevin's analysis,[12] the transverse viscosity was extracted from her SLS data for various polymer and surfactant monolayers. Crilly and Earnshaw have found a finite value of the dynamic transverse viscosity for a monolayer of glycerol monooleate at A/W[18] and also for a bilayer of the same material suspended in water.[19,20] Other authors[10,13,14] studied the same system as Langevin[12] and found no need to invoke the transverse viscosity when fitting their data with the dispersion relation. Recently, we have also found the transverse viscosity to be close to zero at A/W and O/W for a PEO–polystyrene block copolymer.[7]

The controversy over the transverse viscosity may never be resolved experimentally because there is no easy way of comparing it to the corresponding one obtained by other methods. On the other hand, the longitudinal dynamic elasticity obtained by SLS and the static counterpart obtained by the plate method have been extensively compared.[9,11-14] The comparison gives rise to further insight into the dynamic longitudinal elasticity despite its "contamination" by a shear component,[15] while the static elasticity is purely dilational. This comparison so far has been quite qualitative, even with the improvement of experimental precision. This is because the most widely studied monolayer samples such as fatty acids[10-14] have biphasic regions, wherein the comparison of the static and dynamic longitudinal elasticities is complicated by the phase coexistence. PVAc and PEO however give rise to one phase for all surface concentrations; thus a quantitative comparison of the surface elasticities obtained by the two methods can be made.

Experimental Section

Materials. PEO of various molecular weights with M_w/M_n less than 1.05 were from Toyo Soda Co. (supplied by Varian Associates, Sunnyvale, CA). Three samples were used here and they are identified by molecular weights in kilograms per mole. The 145K and 594K samples were dehydrated by evacuation at 10^{-5} Torr for 48 h at room temperature. They were found to be indistinguishable from an undried 252K sample as far as the surface experiments were concerned. PVAc was polymerized by free radical polymerization and purified by reprecipitation in methanol.[21] Only one fraction having a molecular weight of 114K was used for this study. Earlier, it has been shown that there exists no molecular weight dependence for PVAc[21] for SLS experiments in the range of 55K–1150K.

The heptane (Aldrich, 99%) was purifed with 60–100 mesh Florisil magnesium silicate and then doubly distilled. The water used here was house distilled water further purified with a Milli-Q filtering system (Millipore) with one carbon and two ion-exchange filters. Dichloromethane (Aldrich, spectro grade, Gold Label) was used without further purification as the spreading solvent. All glassware and Teflon were cleaned with a sulfuric acid–Nochromix (Godax Labs. Inc., New York) solution.

Methods. Since our experimental methods have been described elsewhere,[7] we present only a brief summary here. Both SLS and static measurements were performed simultaneously in a Langmuir trough milled out of Teflon having the dimensions of 28.5 cm × 11.1 cm × 1.0 cm, enclosed in a Plexiglass box (68 cm × 30 cm × 24 cm) with the relative humidity kept at 70%. For the Wilhelmy plate method, a 1.0 cm × 2.5 cm sandblasted platinum plate and a smaller 0.4 cm × 1.73 cm platimum plate were used for A/W and O/W, respectively. The plates were suspended from a Cahn 2000 electrobalance by a fine stainless-steel wire. The surface temperature was controlled to ±0.1 °C at 25 °C by circulating thermostated water through a glass coil placed at the bottom of the trough. For O/W, another (deeper) Teflon trough (10.8 cm × 10.8 cm × 1.7 cm) was substituted. The temperature was controlled to ±0.1 °C at 25 °C by water circulation through the brass casing of the sample cell. The deeper trough allowed us to immerse the plate completely. The size of the prism, which was used as the light pipe for O/W, limited the thickness of the heptane layer to 0.4 cm; hence unlike for A/W, SLS and static measurements were not performed simultaneously. For the sake of consistency, we did try to perform the experiments sequentially under identical conditions.

For A/W, the polymer was spread from dichloromethane solution and the surface concentration was controlled by a sliding Teflon barrier. Two different methods were used to spread the polymer on the heptane/water interface. The continuous addition method was performed by layering successively small amounts (μL) of a dichloromethane solution of the sample onto the interface. Blank experiments with just dichloromethane were performed to confirm that solvent alone had no effect on the interfacial tension. The other method was to spread the sample onto the air/water interface first and subsequently layer heptane onto the water phase. This method gives more complete spreading in most cases but of course is rather tedious. It is referred to as the single-shot method because the entire procedure must be repeated for each surface concentration.

The SLS instrument and its calibration at A/W have been previously reported.[22] The same instrument was modified by using a 4-cm BK-7 glass equilateral prism as a light pipe to access O/W without being interfered with by the air/oil interface. The instrumental calibration at O/W has been described,[7] hence only the important equations for the frequency width correction will be given here. The calibration method was experimentally verified by correctly determining the interfacial tensions of water and

Table I
Calibration Summary at 25 °C

order	k/cm^{-1}	f_s/Hz	Δf_{obsd}/Hz	Δu_i/mm	Δf_i/Hz	$\Delta f_{s,c}$/Hz	σ_{int}/(dyn/cm)	η/cp
				Air/Water				
4	262	5689	630	0.72	401	374	71.3	0.95
5	323	7821	754	0.635	393	549	72.0	0.92
6	385	10176	1015	0.76	514	755	72.0	0.89
7	445	12597	1200	0.72	523	972	71.6	0.86
							71.97[a]	0.890[a]
				Heptane/Water				
5	335.8	5110	740	0.61	235	665		
6	400.0	6625	950	0.48	201	907	(50.8)	(0.39)
7	460.7	8168	1240	0.67	301	1167		
8	522.7	9856	1540	0.69	330	1470		
							50.8[b]	0.39[c]

[a] Reference 38. [b] Reference 39. [c] Reference 40.

several immiscible organic solvents.[8]

The power spectra obtained on a spectrum analyzer (Nicolet, 444A) were fitted to a Lorenzian profile to obtain a frequency shift, f_s (or peak frequency), and an observed full width at the half-height, Δf_{obsd}, which had reproducibilities of approximately 0.5% and 5%, respectively. Before f_s and Δf_{obsd} can be used in the dispersion relation, the instrumental width Δf_i must be subtracted from Δf_{obsd} by using eq 1 giving the corrected width $\Delta f_{s,c}$.[23]

$$\Delta f_{s,c} = \Delta f_{obsd} - \Delta f_i^2/\Delta f_{obsd} \quad (1)$$

The instrumental width Δf_i is simply due to a finite spread of **k** vectors, and Δf_i is related to the instrument profile Δu_i, which is the diffraction spot full width at half-height in the plane of the photocathode. The method of determining the diffraction spot width for each diffraction order was given previously for A/W[22] and for O/W,[7] and representative values are given in Table I. Following Hård et al.,[23] eq 2 is used to find the instrumental width which is then substituted into eq 1. Here, df_s/dk is experimentally

$$\Delta f_i = 2^{3/2}\pi(df_s/dk)(\cos\theta/R\lambda)\Delta u_i \quad (2)$$

determined by performing the experiment at several **k** vectors, where $k = (2\pi/\lambda)\sin\phi\cos\theta$ and the scattering angle is ϕ. The incident angle measured normal to the interface is θ (64.4°), R is the distance from the interface to the photomultiplier (356.0 cm), and λ is the laser wavelength (He/Ne, 632.8 nm).

Results

In order to contrast the polymer interfacial properties and the SLS technique itself at A/W and O/W, we have performed a series of experiments as a function of polymer surface concentration at both interfaces. Static surface tension measurements using the Wilhelmy plate technique were performed simultaneously with all SLS measurements at A/W; this was imperative in precise calculations of ϵ and κ from the two SLS parameters, f_s and $\Delta f_{s,c}$, because we set the dynamic surface pressure π equal to the static surface pressure π_s. Hence, π_s must be known accurately.

Turning to the results, we present them in order of PVAc and PEO in the following sequence: (1) the SLS results at A/W relative to $\Delta f_{s,c}$ and f_s, (2) the corresponding ones at O/W, and (3) the deduced π from SLS at O/W and the measured π_s with the plate method. At the end of the presentation for each polymer a brief comparison of the results of A/W and O/W will be given. Finally the two samples will be contrasted to conclude this section.

Poly(vinyl acetate). The results of the Lorentzian analysis of SLS spectra at A/W are presented in Figure 1 for PVAc at three different **k** values. A plot of $\Delta f_{s,c}$ vs Γ is shown in Figure 1A. Instead of being monotonic with respect to Γ, there exists a rather complex structure in the plot; in fact there are two prominent maxima, one at 5×10^{-5} mg/cm^2 and the other at 16×10^{-5} mg/cm^2, and the second has a smaller amplitude than the first. The frequency shift f_s vs Γ is shown in Figure 1B. Unlike $\Delta f_{s,c}$, f_s is relatively monotonic with Γ it begins with a value remaining about the same as that of bare water or possibly increasing slightly upward until Γ equals about 4×10^{-5} mg/cm^2 before a rapid decrease sets in. At around $\Gamma = 18 \times 10^{-5}$ mg/cm^2, there is a small bump which is not so obvious in the figure but was confirmed to be above the experimental scatter for all three **k** values. These observations of $\Delta f_{s,c}$ and f_s for PVAc are all in accord with the earlier reports; first by Langevin[12] and second from this laboratory[21] where we have extended the range of Γ well over that of Langevin, resulting in finding the second maximum in $\Delta f_{s,c}$. The interpretations and significance of these findings will be deferred to later. For the moment we continue on with the presentation of the results.

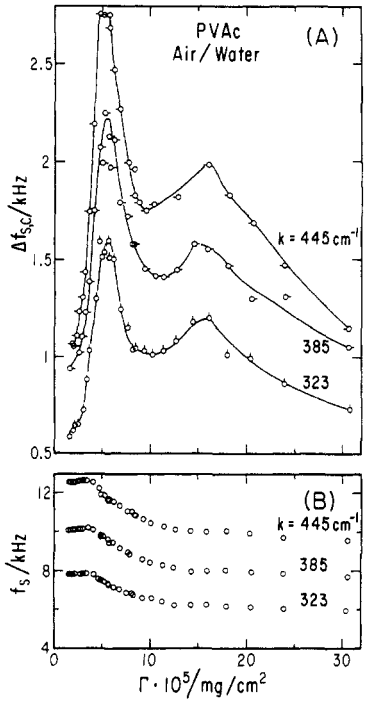

Figure 1. (A) Corrected frequency width vs surface concentration for 114K PVAc at A/W at different **k** vectors. The smooth curves are drawn over the data points to show the trend. (B) Frequency shift vs surface concentration for PVAc at A/W at different **k** vectors.

For PVAc spread at O/W using the continuous addition method, we show $\Delta f_{s,c}$ vs Γ in Figure 2A and f_s vs Γ in Figure 2B. The difference in $\Delta f_{s,c}$ vs Γ for A/W and O/W is rather striking. We see in Figure 2A only a mild maximum at around $(3–5) \times 10^{-5}$ mg/cm^2 amounting to no more than 30–100 Hz above that of the bare water value. Similarly for f_s vs Γ, the difference between the profiles

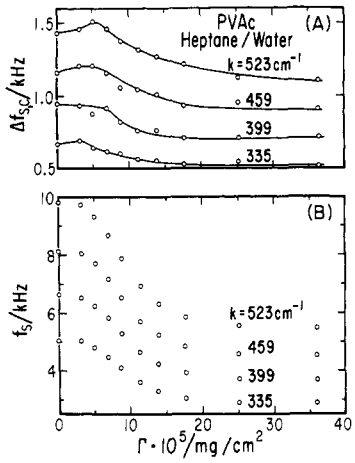

Figure 2. (A) Corrected frequency width vs surface concentration for 114K PVAc at O/W at different **k** vectors. The smooth curves are drawn over the data points to show the trend. (B) Frequency shift vs surface concentration for PVAc at O/W at different **k** vectors.

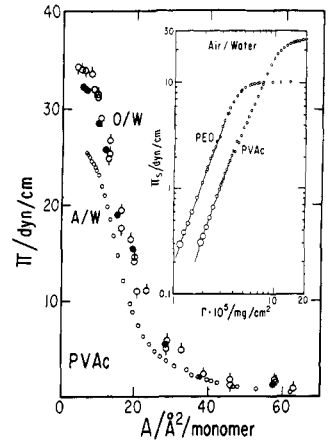

Figure 3. Surface pressure vs A for spread films of 114K PVAc. At A/W (small open circles) the surface pressure was determined by the plate method. At O/W the surface pressure was determined by using SLS and the two different spreading methods indicated are the single shot spreading method (open circles, bips up) and the continuous addition method (open circles, bips down). The static measurements at O/W are represented by filled circles. The inset is a log–log plot of static surface pressure vs surface concentration for PEO and PVAc.

in Figures 1B and 2B is noteworthy; f_s in O/W decreases rapidly starting at $\Gamma = 3 \times 10^{-5}$ mg/cm^2 and the final difference between those of bare water and high coverage limit is much larger than in the A/W case.

As discussed in the introduction, the longitudinal mode decouples from the transverse mode on O/W. As a consequence, the dispersion equation can be solved directly for the two parameters of the complex interfacial tension, $\sigma^*(\Gamma) = \sigma(\Gamma) - i\omega\mu(\Gamma)$, namely, $\sigma(\Gamma)$ and $\mu(\Gamma)$ from the two experimental quantities, f_s and $\Delta f_{s,c}$. The transverse viscosity $\mu(\Gamma)$ so determined has been found to be $(0.0 \pm 0.5) \times 10^{-5}$ g/s, meaning that it is undetectable within our experimental precision. The dynamic surface pressure π was calculated by $\pi = \sigma(0) - \sigma(\Gamma)$ where $\sigma(0)$ is the interfacial tension of the film-free, liquid–liquid interface, and its value from SLS is the same as that by static methods reported in the literature.[8] For PVAc, π was determined from the experiments performed with the two different spreading methods, the single-shot and continuous addition. The results are shown in Figure 3; the data from SLS are given in open circles and they are in turn distinguished by bips according to the spreading method, the single-shot method by bips up and the continuous addition method by bips down. The static Wilhelmy data obtained by the single-shot method are represented by filled circles in the same graph. For the SLS results, the continuous addition method gave the values lower by 0–2 dyn/cm than those obtained by the single-shot method depending on the Γ range. Since π–A curves for the two spreading methods appear to converge at small A, we tentatively attribute the discrepancy to inefficient spreading with the continuous addition method. This could be caused by some PVAc dissolving in the heptane phase before it reaches the interface during the polymer spreading process.

Since the use of SLS in the determination of π for polymers at O/W is relatively unexplored, a comparison of the π–A isotherms obtained by static and dynamic methods is in order. Concentrating only on the data taken with the single-shot method, we infer from Figure 3 that the values of π_s (solid circles) are 1–2.5 dyn/cm lower than π at surface pressures above 15 dyn/cm (e.g., $\pi = 34.0$ dyn/cm and $\pi_s = 32.3$ dyn/cm at $A = 5.5$ Å^2/monomer and $\pi = 31.1$ dyn/cm and $\pi_s = 28.7$ dyn/cm at $A = 9.7$ Å^2/monomer) and at larger values of A the static and dynamic results are almost identical. We ascribe the difference at small A to a systematic inaccuracy in π_s determinations. In fact this is probably due to an overestimate in the determination of the plate constant of the platinum Wilhelmy plate, resulting in an underestimate of π_s. The difference however seems to be so small that we conclude π determined by SLS being the same quantity as that measured by the static method π_s.

We now touch upon the comparison of A/W and O/W. We should first note the theoretical basis of the difference in the dispersion relation explained in the Introduction. Regardless of the nature of the monolayer substance, at A/W the density difference of the two layers is mainly responsible for the efficient coupling of the longitudinal and transverse surface waves, whereas on O/W the negligible density difference essentially decouples the two kinds of surface waves.[17] Hence the same situation will prevail with PVAc monolayers at A/W and O/W. Thus the remarkable contrast noted in the plots of Figures 1A and 2A comes about because there should be a substantial increase in the capillary wave damping, as much as 200% over the bare water value, as the coupling between the two modes becomes more efficient on A/W as Γ is increased, resulting in an increase of ϵ relative to σ. On the other hand, scarcely a noticable increase in the wave damping is seen on O/W since a negligible coupling of the two modes should result in this case. We will return later to why there should be two maxima in the case of A/W. The contrast in the early portion of the π–Γ plots in Figures 1B and 2B also comes about for the same reason as in $\Delta f_{s,c}$. On A/W there should exist a negligible decrease in f_s because of the strong coupling whereas on O/W it decreases from the beginning because there is no coupling, whereby f_s just follows the decrease in σ from the beginning. The subsequent decrease in f_s after the initial constant region on A/W essentially follows the decrease in σ as Γ is increased. In Figure 3, we contrast the surface pressure behaviors on A/W and O/W; the lower series represents the static values of π on A/W. We deduce from the two isotherms that PVAc is slightly more expanded at O/W that at A/W. The limiting surface areas A_0 are determined by extrapolating the linear region of each isotherm to zero surface pressure: the A_0 values of PVAc are 25.1 Å^2/monomer and 28.5 Å^2/monomer on A/W and O/W, respectively. It seems rather plausible that a larger value of A_0 on O/W arises from the fact that the chain excluded

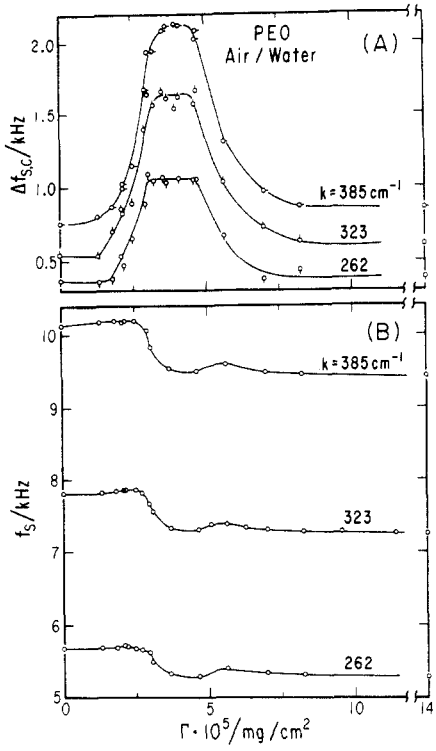

Figure 4. (A) Corrected frequency width vs surface concentration for 252K PEO at A/W. The three different **k** vectors are indicated on the graph. The smooth curves are drawn over the data points to show the trend. (B) Frequency shift vs surface concentration for PEO at A/W at different **k** vectors.

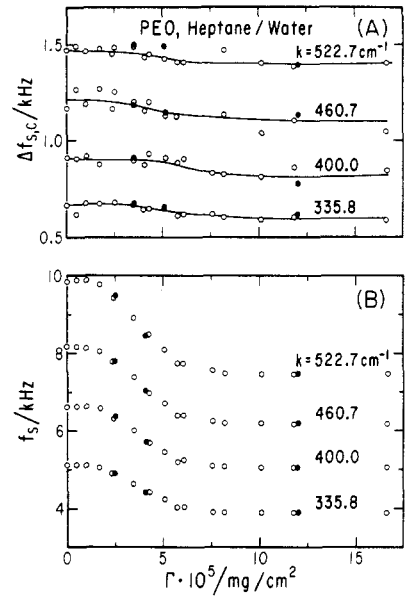

Figure 5. (A) Corrected frequency width vs surface concentration for 252K PEO at O/W at different **k** vectors. The filled circles and open circles are for the single shot and continuous addition spreading methods, respectively, indicating that the SLS results are independent of the spreading method for PEO. (B) Frequency shift vs surface concentration for PEO at O/W. The filled circles and open circles represent the single shot and continuous addition spreading methods, respectively.

volume effect on two-dimensions is manifested for PVAc in the heptane layer. In the language of the traditional monolayer field, one would say that there should be a greater lateral cohesion among polymer segments on A/W such that A_0 ought to be smaller on A/W. We will also return to the inset of Figure 3 after the PEO results are presented.

Poly(ethylene oxide). The corrected frequency width $\Delta f_{s,c}$ of PEO on A/W is plotted against Γ in Figure 4A and the corresponding frequency shift f_s in Figure 4B. The profile of $\Delta f_{s,c}$ shows a broad maximum at around 4×10^{-5} mg/cm^2 while that of f_s shows a broad minimum at the same value of Γ. The conjugate plots on O/W are displayed in Figure 5 where (A) is for $\Delta f_{s,c}$ and (B) is for f_s. The two spreading methods on O/W are distinguished by unfilled and filled circles for the continuous addition and single-shot methods, respectively. The two spreading methods in both graphs are seen to give indistinguishable results within experimental error; this is contrary to the case of PVAc. The magnitude of f_s decreases on A/W and O/W relative to Γ is rather similar to those for PVAc, giving rise to a smaller decrease on A/W and a much larger decrease on O/W.

As in PVAc, π and μ can be calculated unambiguously on O/W by virtue of negligible coupling between the two surface wave modes. Again, μ is shown to be zero within experimental error. The dynamic surface pressure π at O/W is shown in the upper series of Figure 6, where the two spreading methods are represented by different symbols. As stated above the two methods give rise to data sets indistinguishable from each other. The lower series is for the static surface pressure π_s on A/W.

Examining the contrast for PEO at A/W and O/W, it is evident that there is a drastic difference between the two. While there is a large change in $\Delta f_{s,c}$ in Figure 4A, there is almost no change in $\Delta f_{s,c}$ at O/W in Figure 5A except a small decrease. The small maximum at $\Gamma = 2.4$

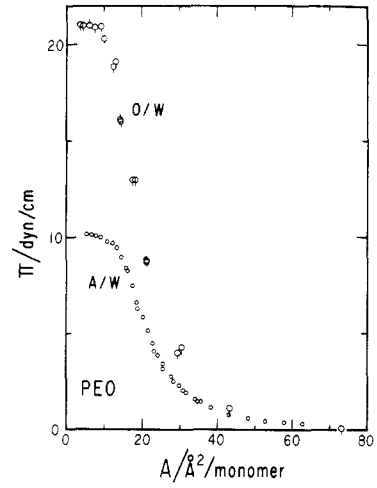

Figure 6. Surface pressure vs area per monomer A for spread films of 252K PEO. The same symbols are used as in Figure 3. No static measurements were performed at O/W.

$\times 10^{-5}$ mg/cm^2 and the bump at 5.5×10^{-5} mg/cm^2 in Figure 4B for f_s at A/W are attributed to the mode coupling. By the same token the large decrease in f_s in Figure 5B reflects no more than the corresponding decrease in the interfacial tension relative to Γ. From the π–A isotherms in Figure 6, we determine the limiting areas A_0 for PEO as 30.5 Å^2/monomer at A/W and 28.5 Å^2/monomer at O/W.

We conclude this section with a brief comparison of PVAc and PEO at A/W and O/W. Surprisingly, A_0 for PEO at A/W is larger than that for PVAc at A/W and O/W even though its monomer unit is smaller. The large A_0 for PEO has been rationalized as the PEO monomers containing adsorbed water molecules[24] which increase the non-hydrated close-packed area from 20.1 Å^2/monomer to 28 Å^2/monomer.[1] The predicted 28 Å^2/monomer is comparable to our A_0 of 30.5 Å^2/monomer and 28.5 Å^2/monomer for PEO at A/W and O/W, respectively.

We now turn to the collapse pressure of the two poly-

mers at both interfaces. They are determined from π–A isotherms in Figures 3 and 6; for PVAc 25 and 34 dyn/cm on A/W and O/W, respectively, and for PEO 10.2 and 21 dyn/cm, respectively. The difference between the two polymers on either interface may be attributed to that of hydrophilicity of the two, PEO being much more hydrophilic than PVAc while both are surface active. The smaller collapse pressure of PEO is ascribed to the segmental desorption into aqueous phase at relatively low surface pressure whereby a substantial chain looping in water is likely to take place. An contrary behavior for PVAc, multilayer formation above the interface, is likely to occur at relatively high surface pressure since it is not water soluble. At A/W such a phenomenon has been shown by Ries and Walker.[25]

Briefly now we return to the static surface pressure π_s dependence on surface concentration Γ on A/W for both polymers. The results are given in double logarithmic plots in the inset of Figure 3. The context of this discussion is the scaling law predictions[26,27] of two-dimensional chains in semidilute regime in "good solvent". PVAc follows a power law, $\pi_s \propto \Gamma^{2.79\pm0.05}$ for $0.3 \leq \pi_s \leq 3.0$ dyn/cm, and PEO follows $\pi_s \propto \Gamma^{2.77\pm0.05}$ for $0.3 \leq \pi_s \leq 3.5$ dyn/cm. Two points should be made. First, the range of the observed power law behavior is about 1 order of magnitude in π_s whereas that of Γ is at best one-half of a logarithmic decade. Secondly, there seems another power law region for PVAc before the collapse pressure is reacted whereas PEO goes over smoothly to the collapse pressure. In an earlier report from this laboratory[21] some reference to this PVAc behavior has been made. Returning to the principal power law regimes for the both polymers, the observed powers close to 2.8 are to be contrasted to the initial des Cloiseaux prediction[27] of 3.0 and 2.85 from the more recent renormalization group prediction.[28] Within experimental error, our results are in accord with 2.85. We should remark that these findings are not new; in fact the earlier determinations of these power law regimes for PVAc[21] and PEO[2,29] are not different from ours.

Discussion

The final section of this paper deals with a discussion of film viscoelastic quantities obtained by the two techniques. As stated earlier, the longitudinal elasticity ϵ and viscosity κ cannot be calculated at O/W while they can at A/W because of the mode coupling. To compare with the dynamic longitudinal elasticity ϵ, the static dilational elasticity ϵ_s is determined from the concentration dependence of π (or π_s).

$$\epsilon_s = \Gamma(d\pi_s/d\Gamma) \tag{3}$$

The same quantity ϵ_s on O/W is also calculated by using eq 3, since the equivalency of π_s and π at O/W have been established, at least for PVAc. In the inset of Figure 7A the comparison of ϵ_s for PVAc at A/W and O/W shows that the static elasticities are very similar in peak position and magnitude. Others[30-32] have also found the similarity of PVAc at A/W and O/W interfaces.

By comparing ϵ_s with $\Delta f_{s,c}$ at A/W, the two peaks in Figure 1A for $\Delta f_{s,c}$ vs Γ can be qualitatively explained. The static elasticity ϵ_s in Figure 7A for PVAc at A/W has its maximum very close to this minimum in $\Delta f_{s,c}$. Referring to theoretical predictions of the effect on ϵ on $\Delta f_{s,c}$,[9] it is seen that the maximum coupling between longitudinal and capillary waves occurs at a reduced elasticity of $\epsilon/\sigma = 0.2$, while at higher values the coupling decreases resulting in decrease of $\Delta f_{s,c}$. Thus, as ϵ increases with Γ, it reaches first to $\epsilon/\sigma = 0.2$ where $\Delta f_{s,c}$ maximizes. Further increase in Γ causes ϵ/σ to exceed 0.2, bringing about a decrease in $\Delta f_{s,c}$. At a maximum attainable value of ϵ/σ beyond 0.2, we should expect a minimum value of $\Delta f_{s,c}$ since upon a further increase in Γ, ϵ/σ starts to decrease, increasing $\Delta f_{s,c}$ once again. This will bring about ϵ/σ to equal 0.2 once again, and at that point, we should have the second maximum of $\Delta f_{s,c}$. Beyond here ϵ/σ will decrease as Γ increases, which entails a further decrease in $\Delta f_{s,c}$. The reason for the second maximum to have a smaller magnitude than the first one arises from the fact that the dilational viscosity κ increases simultaneously with Γ whereby the magnitude of maximum is attentuated by κ as ϵ/σ reaches 0.2 for the second time. By the same reasoning, PEO should have one maximum because ϵ/σ does not reach beyond 0.2.

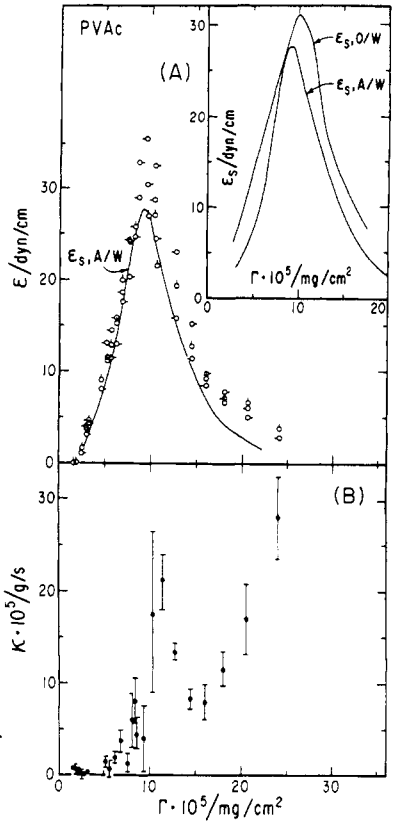

Figure 7. (A) Surface elasticity vs surface concentration for 114K PVAc at A/W. The static dilational elasticity is represented by the continuous curve, and the dynamic longitudinal elasticity obtained by SLS is represented at different **k** vectors as k = 323 cm^{-1} (Ó), k = 385 cm^{-1} (O-), and k = 445 cm^{-1} (-O). In the inset a comparison of the static dilational elasticities at A/W and O/W is shown. (B) Surface longitudinal viscosity vs surface concentration for PVAc at A/W. The bars represent one standard deviation calculated from among the three **k** vectors.

If we are to combine these phenomenological explanations for two maxima in PVAc with an earlier speculations[21] about the five chain conformational states on A/W, it could be said that each milestone event in the five-state model now accompanies a specific ϵ/σ value. Alternatively, we can restrict ourselves to the phenomenology without proposing any model for the conformational states. Clearly, we have no evidence to refute the five-state model.

For PEO spread at O/W with the continuous addition method, ϵ_s is calculated and presented as the smooth curve labeled ϵ_s, O/W which is in turn compared with ϵ_s, A/W in Figure 8A. The static elasticities have the same peak position, but the magnitude of ϵ_s in Figure 8A at O/W is almost twice that of ϵ_s, A/W. Although seemingly simple, ϵ_s is not a well-substantiated quantity because there are few experimental techniques with which comparison can be made.[33] The SLS technique provides an analogous

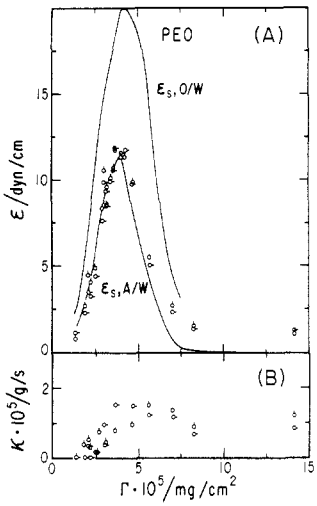

Figure 8. (A) Surface elasticity vs surface concentration for PEO at A/W and O/W. The static dilational elasticities are represented by the upper and lower continuous curves for O/W and A/W, respectively. The longitudinal elasticities at A/W obtained by SLS are represented at different **k** vectors as k = 323 cm^{-1} (○) and k = 385 cm^{-1} (○-). (B) Surface longitudinal viscosity vs surface concentration using the same symbols as in part A.

elastic quantity, the dynamic longitudinal elasticity ϵ. Langevin[12] earlier used a curve fitting procedure to extract π, μ, ϵ, and κ from the two experimental quantities f_s and $\Delta f_{s,c}$ as have Kawaguchi et al.[21] Langevin was forced to invoke a finite μ in fitting her data in some concentration regions, but others did not have this difficulty[7,9,10,13,14] as was the case for this work. The calculation of ϵ and κ was made by substituting f_s and $\Delta f_{s,c}$ in the dispersion relation and assuming $\pi = \pi_s$ and $\mu = 0$. A comparison is made of ϵ_s and ϵ so calculated in Figure 7A for PVAc at A/W. The curve designated as ϵ_s, A/W represents the static values calculated according to eq 3. The dynamic elasticity is represented by open circles with bips in Figure 7A. For PVAc in Figure 7A, ϵ is very close to ϵ_s up to somewhere between Γ = 9 and 16 × 10^{-5} mg/cm^2, after which ϵ becomes systematically larger than ϵ_s. A comparison between ϵ_s, which was calculated from the π–Γ isotherm using eq 3 and the dynamic ϵ, is not a valid one above Γ = 10 × 10^{-5} mg/cm^2 since eq 3 is not applicable at the higher concentrations where the PVAc segments are presumably leaving the interface.

The values of ϵ for PEO at A/W follow the same trend as those for PVAc except both ϵ and ϵ_s are smaller in magnitude. In Figure 8A, ϵ and ϵ_s are indistinguishable up to the peak in the elasticity at 3.9 × 10^{-5} mg/cm^2. Somewhere around this point, however, ϵ becomes systematically larger than ϵ_s. The agreement between ϵ and ϵ_s for both polymers may be fortuitous because of the assumptions made; nevertheless some mention should be made of this important comparison. The longitudinal elasticity ϵ is predicted to be a combination of dilational and shear components[15] while ϵ_s is purely dilational. However, since ϵ_s and ϵ are almost identical at the lower concentration range, we would conclude that the shear component may be negligible. A similar conclusion has been drawn previously.[33]

The error associated with the determination of ϵ is estimated as follows. Given the uncertainties in f_s, $\Delta f_{s,c}$, and π of 0.5%, 5%, and 0.2 dyn/cm, respectively, the error in the calculated ϵ for PEO is ±0.5 dyn/cm and for PVAc is ±2 dyn/cm. Both of these error values are reasonable upper estimates, with ϵ generally being more precise at most concentrations.

The surface longitudinal viscosity κ was also calculated for both polymers by using the same assumptions as for the calculation of ϵ. In Figure 7B the results of this calculation are shown for PVAc. The error bars represent one standard deviation among different **k** vectors. The error due to uncertainty in f_s, $\Delta f_{s,c}$, and π is hard to estimate because κ is very sensitive to f_s and π. For example, changing f_s by 20 Hz changes κ from 3 to 9 × 10^{-5} g/s at Γ = 8.3 × 10^{-5} mg/cm^2. From Figure 7B it is evident that there is a maximum in κ between 10 and 12 × 10^{-5} mg/cm^2. We are not sure what this maximum represents, but it occurs near the closely packed monolayer state in a manner similar to the maximum for ϵ.

Because of experimental difficulties in obtaining reliable surface viscosities using any method, a brief comparison of κ with some literature values for PVAc is in order. Most surface viscosity experiments measure the shear component, and Joly[34] has summarized the temperature and molecular weight dependence of the surface shear viscosity of a few polymers. Surface shear viscosities determined by the oscillation damping method at 25 °C for 220K PVAc are 34 × 10^{-5} g/s[34,35] at Γ = 9 × 10^{-5} mg/cm^2 which are similar to our value of κ = 10 × 10^{-5} g/s for 114K PVAc at Γ = 10 × 10^{-5} mg/cm^2 (Figure 7B). At higher concentrations, their values increase rapidly to 520 × 10^{-5} g/s at Γ = 12 × 10^{-5} mg/cm^2 while our values of κ never rise above 30 × 10^{-5} g/s. The surface shear viscosity values also rose monotonically with Γ while our κ decreases starting at Γ = 12 × 10^{-5} mg/cm^2 and finally minimizes at about Γ = 16 × 10^{-5} mg/cm^2. The discrepancy even in the general trend may be attributed to the different techniques used; however, further SLS investigations are needed to delineate the molecular weight and temperature dependence of κ.

For PEO κ was calculated, and the results are displayed in Figure 8B. The magnitude of κ is extremely small compared to most polymers[12,21] and surfactants[7,9-13] studied previously. The calculation of κ for PEO is quite precise with a 0.5%, 5%, and 0.2 dyn/cm error in f_s, $\Delta f_{s,c}$, and π, respectively; this gives rise to a maximum uncertainty of 0.5 × 10^{-5} g/s error for κ. From Figure 8B it is evident that κ is zero at Γ = 1.3 × 10^{-5} mg/cm^2 and that it increases to between 1.0 and 1.5 × 10^{-5} g/s at 3.5 × 10^{-5} mg/cm^2 and remains between these past the collapse pressure of 10.2 dyn/cm. This can be contrasted with a low molecular weight poly(styrene)–PEO block copolymer where κ increased to over 100 × 10^{-5} g/s at pressures above the collapse pressure of PEO. This means that the poly(styrene) segment–segment cohesion probably contributes to the large κ. Concurrent with this idea, the reason κ is ten times larger for PVAc than PEO might be that PVAc exhibits greater polymer–polymer cohesion at the A/W interface.

A recently developed theory for polymers at liquid interfaces[36] has been applied to PEO and PVAc data at A/W and O/W.[37] By fitting π–A curves for PEO, it was found that the Einstein characteristic temperature for the transverse oscillation of the layer of segments attached to the interface was larger at O/W than A/W and that the close-packed area was smaller at the O/W.[37] The larger Einstein characteristic temperature indicates that attraction at the O/W is greater than that at the A/W. Similar calculations were performed on PVAc at A/W and O/W[37] showing that all the parameters were about the same at both interfaces, as was found earlier by Gabrielli and Puggelli[32] using a different theory for PVAc at A/W and O/W.

Summary

By combining SLS and static Wilhelmy plate mea-

surements at A/W and O/W interfaces, spread films of PEO and PVAc have been studied. The polymer films served as model systems to compare the capabilities of the SLS technique at A/W and O/W. Several conclusions were drawn from the comparison. At O/W, the longitudinal modes do not couple efficiently with the transverse modes of the surface waves. This makes the technique ideal for the determination of the interfacial tension and, hence, the surface pressure, since the surface longitudinal elasticity ϵ and viscosity κ have almost no influence on the capillary wave motion. The surface pressure obtained by using SLS was found to agree with the static surface pressure over the entire concentration range within experimental error for PVAc at O/W. An umambiguous calculation of the transverse viscosity μ was also made possible because of this decoupling and was found to be less than 5×10^{-6} g/s for the entire concentration range at O/W for both PVAc and PEO.

In contrast, at A/W a strong coupling of longitudinal and capillary waves allowed us to calculate both the longitudinal elasticity and viscosity, *assuming* $\mu = 0$. For both PEO and PVAc the dynamic and static surface elasticities were in agreement up to the maximum in elasticity. Since the static elasticity is purely dilational, we conclude that in this region the shear contribution is negligible. At concentrations above this maximum the dynamic elasticity is slightly larger than the static possibly due to a partial desorption of polymer segments. The longitudinal viscosity was found to be almost ten times greater for PVAc than PEO and the viscosity calculation for PVAc is the same order of magnitude as that calculated previously.[12,21]

Acknowledgment. This work was in part supported by the Research Committee of the University of Wisconsin—Madison, the University Exploratory Research Program of the Procter and Gamble Co., and Kodak Research Laboratories. We are most grateful to our colleagues, Professors George Zografi and Hyungsuk Pak and Drs. Yen-Lane Chen, Masahito Sano, and Kyung-Hwa Yoo, for fruitful discussions.

Registry No. PVAc, 9003-20-7; PEO, 25322-68-3.

References and Notes

(1) Shuler, R. L.; Zisman, W. A. *J. Phys. Chem.* **1970**, *71*, 1523.
(2) Kawaquchi, M.; Komatsu, S.; Matsuzumi, M.; Takahashi, A. *J. Colloid Interface Sci.* **1984**, *102*, 356.
(3) Glass, J. E. *J. Phys. Chem.* **1968**, *72*, 4459.
(4) Glass, J. E. *J. Polym. Sci., Part C* **1971**, *34*, 141.
(5) For a recent review of the literature see: Molyneux, P. *Water Soluble Synthetic Polymers: Properties and Behavior*; CRC Press: Boca Raton, FL, 1984; Vol. II, p 179.
(6) For a review of work done before 1960 see: Danielli, J. F., Pankhurst, K. G. A., Riddiford, A. C., Eds. *Surface Phenomena in Chemistry and Biology*; Pergamon: London, 1958; p 23.
(7) Sauer, B. B.; Yu, H.; Tien, C.-F.; Hager, D. F. *Macromolecules* **1986**, *20*, 393.
(8) Sauer, B. B.; Chen, Y.-L., Zografi, G.; Yu. H. *Langmuir* **1986**, *2*, 683.
(9) Hård, S.; Löfgren, H. *J. Colloid Interface Sci.* **1977**, *60*, 529.
(10) Byrne, D.; Earnshaw, J. C. *J. Phys. D: Appl. Phys.* **1979**, *12*, 1145.
(11) Langevin, D.; Griesmar, C. *J. Phys. D: Appl. Phys.* **1980**, *13*, 1189.
(12) Langevin, D. *J. Colloid Interface Sci.* **1981**, *80*, 412.
(13) Hård, S.; Neuman, R. D. *J. Colloid Interface Sci.* **1981**, *83*, 315.
(14) Chen, Y. L.; Sano, M.; Kawaguchi, M.; Yu, H.; Zografi, G. *Langmuir* **1986**, *2*, 349.
(15) Mann, J. A. *Langmuir* **1985**, *1*, 10.
(16) Goodrich, F. C. *J. Phys. Chem.* **1962**, *66*, 1858.
(17) Lucassen-Reynders, E. H.; Lucassen, J. *Adv. Colloid Interface Sci.* **1969**, *2*, 347.
(18) Crilly, J. F.; Earnshaw, J. C. In *Biomedical Applications of Laser-Light Scattering*; Sattelle, D. B., Lee, W. I., Ware, B. R., Eds.; Elsevier/North Holland: Amsterdam, 1982; p 123.
(19) Crilly, J. F.; Earnshaw, J. C. *Biophys. J.* **1983**, *41*, 211.
(20) Crawford, G. E.; Earnshaw, J. C. *Biophys. J.* **1986**, *49*, 869.
(21) Kawaguchi, M.; Sano, M.; Chen, Y.-L.; Zografi, G.; Yu, H. *Macromolecules* **1986**, *19*, 2606.
(22) Sano, M.; Kawaguchi, M.; Chen, Y.-L.; Skarlupka, R. J.; Chang, T.; Zorgrafi, G.; Yu, H. *Rev. Sci. Instrum.* **1986**, *57*, 1158.
(23) Hård, S.; Hamnerius, Y.; Nilsson, O. *J. Appl. Phys.* **1976**, *47*, 2433.
(24) Rosch, M. *Kolloid-Z.* **1956**, *78*, 147.
(25) Ries, H. E; Walker, D. C. *J. Colloid Sci.* **1961**, *16*, 361.
(26) de Gennes, P. G. *Scaling Concepts in Polymer Physics*; Cornell University Press: Ithaca, NY; 1979.
(27) des Cloiseaux, J. *J. Phys. (Paris)* **1975**, *36*, 1199.
(28) Le Guillou, J. C.; Zinn-Justin, J. *Phys. Rev. Lett.* **1977**, *39*, 95.
(29) Kawaguchi, M.; Yu, H., to be submitted for publication.
(30) Crisp, D. J. *J. Colloid Sci.* **1946**, *1*, 49.
(31) Schick, M. J. *J. Polym. Sci.* **1957**, *25*, 465.
(32) Gabrielli, G.; Puggelli, M. *J. Colloid Interface Sci.* **1971**, *35*, 460.
(33) Lucassen-Reynders, E. H. In *Anionic Surfactants*; Lucassen-Reynders, E. H., Ed.; Marcell Dekker: New York, 1981; Vol. 11, p 173.
(34) Joly, M. In *Surface and Colloid Science*; Vol. 5; Matijevic, Ed.; Interscience: New York, 1972; Vol. 5, p 91.
(35) Isemura, T.; Fukuzuka, K. *Mem. Inst. Sci. Ind. Res., Osaka Univ.* **1956**, *13*, 137.
(36) Pak, H.; Yu, H., submitted for publication in *Macromolecules*.
(37) Pak, H.; Sauer, B. B.; Yu, H., to be submitted for publication.
(38) Weast, R. C., Ed. In *CRC Handbook of Physics and Chemistry*; 56th ed.; CRC Press: Cleveland, OH, 1975.
(39) Aveyard, R.; Haydon, D. A. *Trans. Faraday Soc.* **1965**, *61*, 2255.
(40) Fleischer, D. In *Polymer Handbook*; Brandrup, J., Immergut, E. H., Eds.; Wiley: New York, 1975.